Available on CMS information server

CMS CR -2022/270

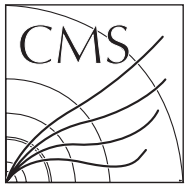

The Compact Muon Solenoid Experiment

Conference Report

Mailing address: CMS CERN, CH-1211 GENEVA 23, Switzerland

02 December 2022 (v3, 14 December 2022)

Characterization of 3D pixel sensors for the CMS upgrade at the High Luminosity LHC

Mauro Dinardo for the CMS Collaboration

Abstract

The High Luminosity upgrade of the CERN Large Hadron Collider (HL-LHC) calls for an upgrade of the CMS tracker detector to cope with the increased radiation fluence, 1.9×10^{16} n_{eq}/cm^2 (1 MeV equivalent neutrons) for the innermost layer, while maintaining the excellent performance of the existing detector. An extensive R and D program, aiming at using 3D silicon pixel sensors, has been put in place by CMS in collaboration with FBK (Trento, Italy) and CNM (Barcelona, Spain) foundries. The basic 3D pixel cell sizes is 25×100 μm^2, with one central readout electrode to be connected to the readout chip. In this presentation results obtained in beam test experiments before and after irradiations, up to $\sim 2.6 \times 10^{16}$ n_{eq}/cm^2, will be reported. The sensors were read out by the RD53A chip, a prototype version of the 65 nm CMOS technology pixel readout chip which will be adopted to read out the CMS pixel detector at HL-LHC.

Presented at *Vertex2022 The 31st International Workshop on Vertex Detectors*

Characterization of 3D pixel sensors for the CMS upgrade at the High Luminosity LHC

Mauro Dinardo[1] on behalf of the CMS collaboration

[1]*Universitadègli Studi di Milano - Bicocca, Milano, Italy*

E-mail: mauro.dinardo@cern.ch

(Received December 5, 2022)

The High Luminosity upgrade of the CERN Large Hadron Collider (HL-LHC) calls for a replacement of the CMS tracker detector to cope with the increased radiation fluence, 1.9×10^{16} n_{eq}/cm^2 (1 MeV equivalent neutrons) for the innermost layer, while maintaining the excellent performance of the detector. An extensive R&D program, aiming at using 3D silicon pixel sensors, has been put in place by CMS in collaboration with FBK (Trento, Italy) and CNM (Barcelona, Spain) foundries. The basic 3D pixel cell size is 25×100 μm^2, with one centrally located electrode connection to the readout chip. In this presentation results obtained in beam test experiments before and after irradiations, up to $\sim 2.6 \times 10^{16}$ n_{eq}/cm^2, will be reported. The sensors were read out by the RD53A chip, a prototype version of the 65 nm CMOS technology pixel readout chip planned for the HL-LHC CMS pixel detector.

KEYWORDS: Silicon, pixel, HL-LHC, CMS

1. Introduction

In the coming years, the LHC accelerator will be upgraded to enable an instantaneous peak luminosity of 7.5×10^{34} cm^{-2} s^{-1}, the so-called High Luminosity LHC (HL-LHC) [1], which is expected to run at a center-of-mass energy of 14 TeV and with a bunch spacing of 25 ns. This will allow the CMS experiment [2] to collect an integrated luminosity of the order of 400 fb^{-1} per year and up to 4000 fb^{-1} during the HL-LHC projected lifetime of ten years. The HL-LHC upgrade is accompanied by an upgrade program of the CMS experiment ("phase 2" upgrade), to maintain the excellent performance of the detector and to allow physicists to fully profit from the HL-LHC luminosity, despite the challenging radiation levels and operating conditions. A detailed description of the CMS upgrade can be found in the Tracker Technical Design Report [2]. The CMS phase-2 tracker detector is divided into two main systems: the Inner Tracker (IT) and the Outer Tracker (OT). The IT, illustrated in Fig. 1, is composed of $\sim$ 2 billion pixels, corresponding to an area of $\sim$ 5 m^2 of silicon, with a pseudorapidity coverage up to $|\eta| \simeq 4$.

One of the most critical geometrical parameters in the development of the sensors is the distance between the electrodes that generate the electric field for charge collection. It is well known that to operate silicon sensors at high irradiation fluences, the input of the pre-amplifier should be connected to the electrode that collects electrons (the faster carriers). Furthermore, to keep the bias voltage as low as possible while preserving most of the signal, the distance between opposite-sign electrodes should not exceed a few times the electron mean-free-path at saturation velocity. The best choice is a n^+-on-p sensor as this avoids type-inversion of the bulk and is less expensive than n^+-on-n since it allows for a single-side process, having both the pixel implants and the guard-rings on the same side. The CMS baseline choice is to replace the barrel layer closest to the beamline at an integrated fluence of 1.9×10^{16} n_{eq}/cm^2, which will occur after approximately 6 years of operation (coinciding with the

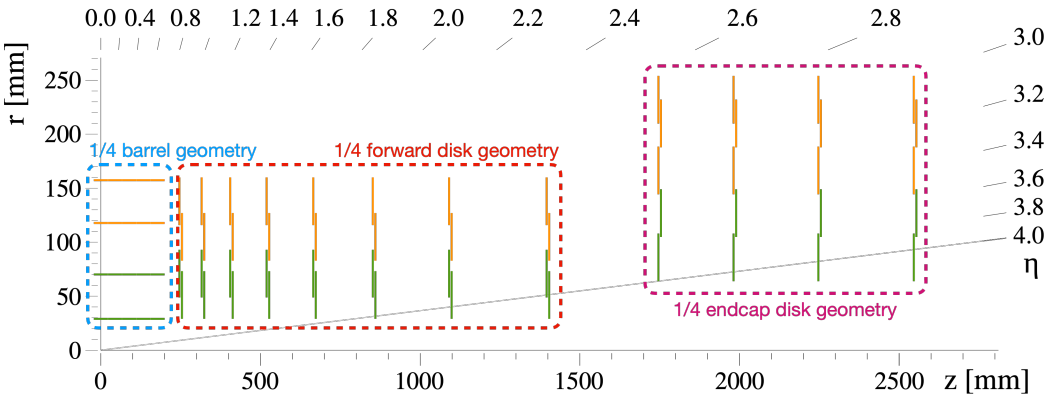

Fig. 1. Schematic view of one quarter of the Inner Tracker geometry. The three main sub-detectors are highlighted, i.e., barrel, forward, and endcap. Green and orange stand for 1×2 and 2×2 readout chip modules, respectively.

end of "Run 5").

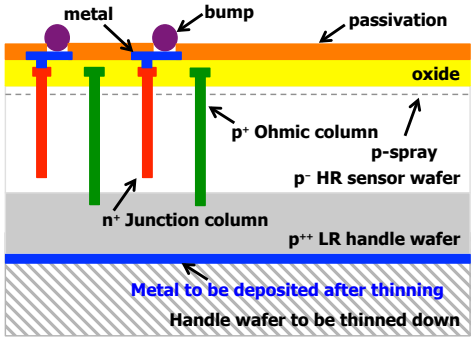

Fig. 2. Cross-section of a typical FBK/CNM 3D silicon pixel sensor. Shown are the high resistivity (HR) and low resistivity (LR) layers, together with the p^+ Ohmic columns (green), and the n^+ junction columns (red) [9].

Two different technological solutions are available: planar sensors, where the electrodes are parallel to the sensor surface, and 3D sensors, where the electrodes are orthogonal to the sensor surface. In the first case the distance between the electrodes is fixed by the sensor's active layer thickness, in the second case it is limited by the layout and the technological process used to fabricate the sensor. To keep the pixel occupancy at per mille level at the expected HL-LHC peak luminosity, and to improve the spatial resolution, the foreseen pixel cell size is 25×100 μm^2. Square-profile pixels (50×50 μm^2) in the endcap and forward regions of the detector have been also studied. Marginal gains were observed in the simulated reconstruction of high-level objects (jets) and algorithms (jets tagging) so this option was not pursued. Though planar sensors are the baseline choice for the Inner Tracker, they cannot be used for layer 1 of the barrel, because there is a risk of thermal run-away for the planar sensors. Therefore, for barrel layer 1 we foresee the use of 3D sensors with the same pitch as the planar ones.

Sensors from the most recent productions were designed to be bonded to the RD53A [3] ReadOut Chip (ROC), which is the first prototype of the CMS pixel ROC for HL-LHC. The RD53A pixel matrix has 400 columns and 192 rows, and the cell size is 50×50 μm^2.

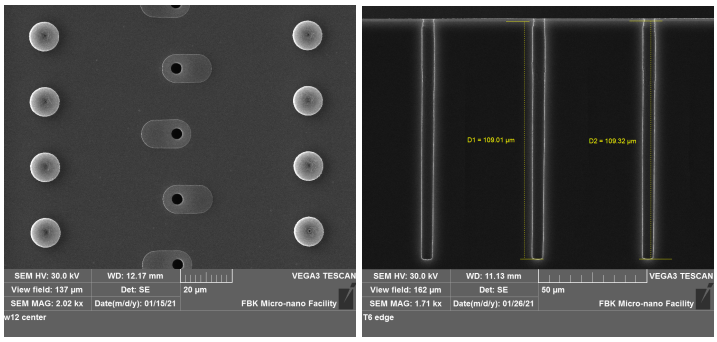

Fig. 3. Electron microscope images of the bump pads (left) and the junction columns (right). The junction columns in the left image have not yet been filled with polysilicon.

Irradiation of the modules took place at the Karlsruhe Institute of Technology [7] using 25 MeV protons, resulting in a uniform irradiation profile, and the CERN Proton Synchrotron using 24 GeV protons, resulting in a non-uniform irradiation profile. Test beam campaigns have been performed both at DESY [4] and at CERN test beam facilities using 5.2 GeV electron and 120 GeV pion beams, respectively.

2. 3D silicon sensors

The 3D silicon sensors described in this article were manufactured by two companies: Fondazione Bruno Kessler [5] (FBK) and Centro Nacional Microtecnologia [6] (CNM). Both companies use two silicon wafers, one with low and one with high resistivity, bonded together with the Direct Wafer Bonding technique developed by ICEMOS [8]. The high resistivity layer has a nominal thickness of 150 μm and a resistivity greater than 3 kOhm·cm, while the low resistivity layer has an initial thickness of 500 μm, which is then thinned down to 50-100 μm, and a resistivity of 0.1-1 kOhm·cm. The columns are produced by a single-side Deep Reactive Ion Etching (DRIE) process, which is less expensive than a double-side one. The main differece between FBK and CNM processes is the column diameter, which is 5 μm for FBK and 8 μm for CNM. Figure 2 shows a sketch of the 3D geometry in which both the high resistivity layer, i.e., active layer, and the low resistivity layer are represented.

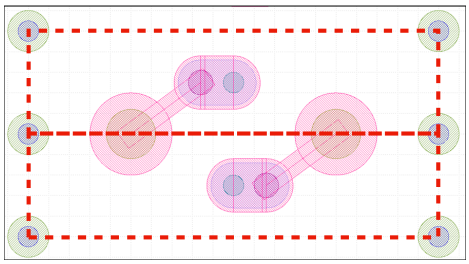

Fig. 4. Schematic view of two adjacent pixel cells, together with the routing from the bump pads, between cells, to the junction columns, near the center of the pixel cells.

Two electron microscope images are presented in Fig. 3: the first one shows the silicon wafer from the top and hence one can see the bump pads, the second one shows a cross-section of the wafer from which one can see the junction columns. All pixel cells are 1E type, i.e., with one junction

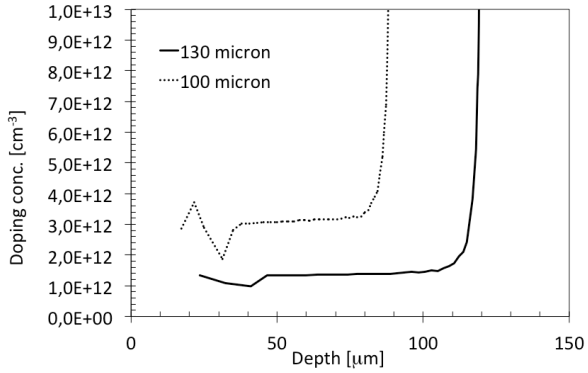

Fig. 5. Plot showing the trend of the measured doping concentration as a function of the depth for 100 and 130 μm thick silicon sensors. The low resistivity layers are effectively $\sim$ 10 μm less thick owing to Boron diffusion from the carrier wafer [10].

column electrode per pixel. The column length can be either 125 $\pm$ 5 μm or 110 $\pm$ 5 μm depending on the design choice. (It will be made clear when presenting the results which design was used.) In order to match the readout chip pitch a special routing, shown in Fig. 4, was adopted.

Though the active layer thickness is 150 μm by design, the actual thickness is $\sim$ 10 μm shorter owing to Boron diffusion from the wafer carrier, i.e., from the low resistivity layer, as shown in Fig. 5; therefore the expected Landau Most Probable Value (MPV) is $\sim$10 190 electrons for a nominal 150 μm thick active layer sensor.

3. Testbeam setup

Both the DESY and CERN testbeam setups make use of the European telescope design (EUDET). The telescope feature 5 or 6 pixel planes, depending on the site, and they are based on the Mimosa26 chip, which has 18.4 μm pitch square pixels, with 1152 columns and 566 rows. The telescope estimated resolution is $\sim$ 2 μm for each coordinate [11].

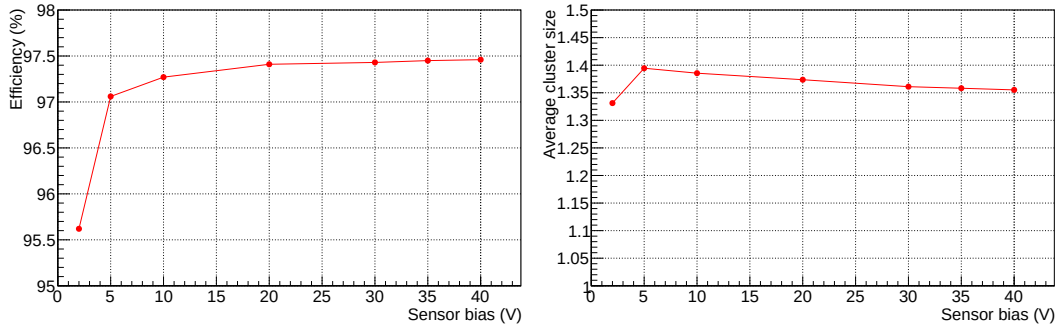

Fig. 6. Plots showing the efficiency (left) and average cluster size (right) for unirradiated CNM sensors as a function of the sensor bias voltage. The average threshold was 2500 electrons and tracks with a normal incidence angle were used.

The sensors were bump-bonded to the RD53A readout chip made in the 65 nm CMOS technology, and featuring 3 frontends, out of which CMS will use the "linear" one (192 rows $\times$ 136 columns).

The chip can read out multiple bunch crossings and a global threshold can be set with a per-pixel 4-bit threshold trimming. The charge is measured with a Time-over-Threshold technique and digitized with a 4-bit ADC.

4. Unirradiated sensors

Measurements of efficiency and cluster size as a function of the sensor bias voltage for unirradiated CNM sensors are shown in Fig. 6. The data were measured with normal incidence tracks and with an average threshold of 2500 electrons. (By mistake we were reading just one bunch crossing, which resulted in a relatively high in-time threshold.) The efficiency peaks at 97.5% because of the Ohmic column inefficiency, the 4-pixel sharing, and the relatively high threshold.

5. Sensor irradiated at 1.5×10^{16} n_{eq}/cm^2

An FBK sensor, with junction column length of 110 ± 5 μm, was irradiated at KIT up to 1.5×10^{16} n_{eq}/cm^2. Figure 7 shows the efficiency maps (left) and cluster size maps (right) at two sensor bias voltages, 50 V and 150 V, for the upper and lower plots, respectively. The lower efficiency map confirms that at 150 V the sensor was fully depleted.

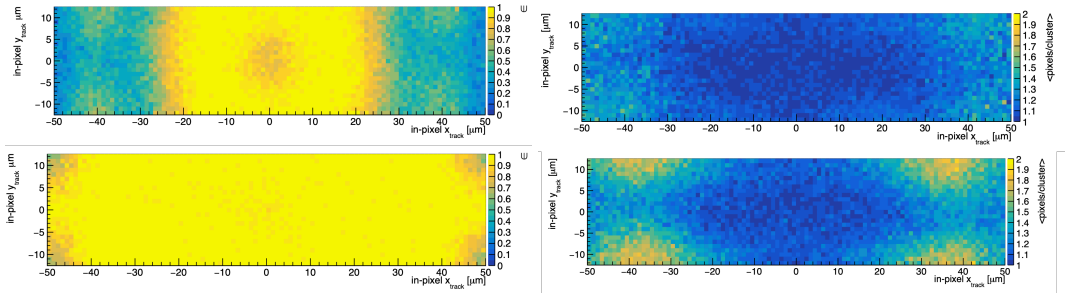

Fig. 7. Efficiency maps (left) and average cluster size maps (right) for irradiated FBK sensors at 1.5×10^{16} n_{eq}/cm^2. Both observables were measured at a sensor bias voltage of 50 and 150 Volts, shown in the upper and lower maps, respectively. The average threshold was 1400 electrons and tracks with normal incidence angle were used.

Figure 8 shows the charge distribution measured at 120 V after applying the calibrations to all pixel cells. From the distributions measured at different sensor bias voltages we extracted the MPV of the charge by a fit with a Landau convoluted with a Gaussian.

With tracks at normal incidence angle we measured the efficiency and Landau MPV as a function of the sensor bias voltage, as reported in Fig. 9. Moreover, for every voltage step we also measured the percentage of masked pixels. We masked pixels having a noise occupancy greater than 10^{-6}. The maximum tolerated percentage of masked pixels is chosen to be 1%. We are investigating the cause of the relatively high number of masked pixels. The number of noisy pixels can be lowered by increasing the occupancy threshold, but as backup plan a replacement of barrel layer 1 could take place earlier than anticipated.

We measured the efficiency and resolution as a function of the track incidence angle as reported in Fig. 10. The efficiency decreases at 20 degrees because the tracks traverse less active pixel material. To evaluate the sensor resolution we subtracted in quadrature the telescope resolution of 3.8 μm, computed as the larger of the residuals for the two planes closest to the Detector Under Test (DUT). The resolution for a digital readout is expected to be $25/\sqrt{(12)} \simeq 7.2$ μm, while the optimal resolution

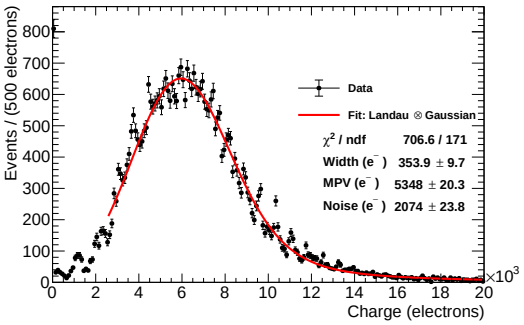

Fig. 8. Charge distribution for irradiated FBK sensors at 1.5×10^{16} n_{eq}/cm^2, measured at 120 V. Parameters from a fit of a Landau distribution convoluted with a Gaussian distribution are shown in the legend. The average threshold was 1400 electrons and tracks with normal incidence angle were used.

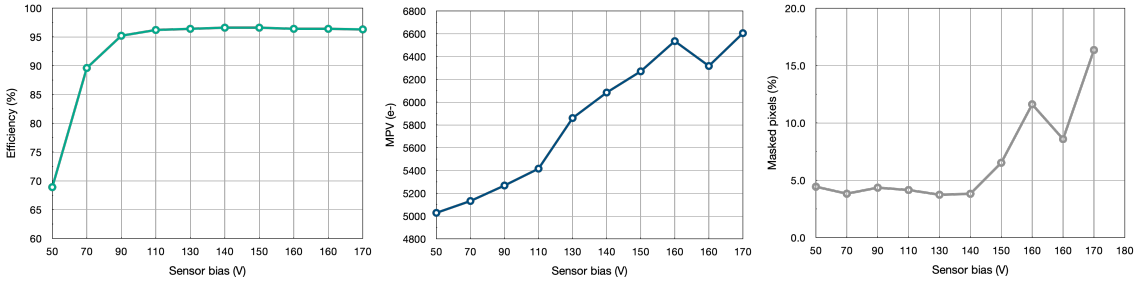

Fig. 9. Efficiency (left), Landau distribution Most Probable Value (MPV, center), and percentage of masked pixels (right) for irradiated FBK sensors at 1.5×10^{16} n_{eq}/cm^2, as a function of the sensor bias voltage. The efficiency does not include the masked pixels. The average threshold was 1400 electrons but for the last two points a threshold of 1500 electrons was used.

is expected to occur at arctan(25/140) $\simeq$ 10 degrees, where 25 μm is the pitch and 140 μm is the actual active layer thickness.

6. Sensor irradiated at 1.8×10^{16} n_{eq}/cm^2

An FBK sensor, with junction column length of 110 ± 5 μm, was irradiated at KIT up to 1.8×10^{16} n_{eq}/cm^2. Figure 11 shows the efficiency and percentage of masked pixels as a function of the sensor bias voltage. We masked pixels with a noise occupancy greater than 2×10^{-5}. The efficiency reaches 98% with a track incidence angle of 12 degrees.

7. Sensor irradiated at $2.1 - 2.6 \times 10^{16}$ n_{eq}/cm^2

Two FBK sensors, each with junction column length of 110 ± 5 μm, were irradiated at CERN up to 2.1 and 2.6×10^{16} n_{eq}/cm^2. Since the irradiation profile was not uniform, we had to extract the irradiation fluence from an aluminum foil placed on the sensor surface during the irradiation campaign. The foil was then divided into 8 pieces from which we measured the activity. The data were then fit with a bivariate Normal distribution without a correlation term, and with constraints on both widths and on the position along the rows. Thanks to the fit profile we were able to define a Region Of Interest (ROI) for each sample in which the irradiation was uniform. We measured average

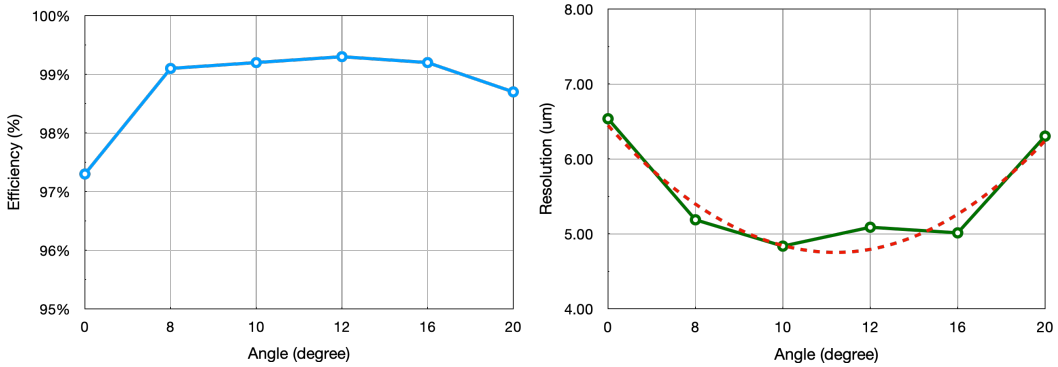

Fig. 10. Efficiency (left) and resolution (right) for irradiated FBK sensors at 1.5×10^{16} n_{eq}/cm^2, as a function of the track incidence angle. The resolution plot includes a fit from a second-degree polynomial. The average threshold was 1400 electrons and the sensor bias voltage was 120 V.

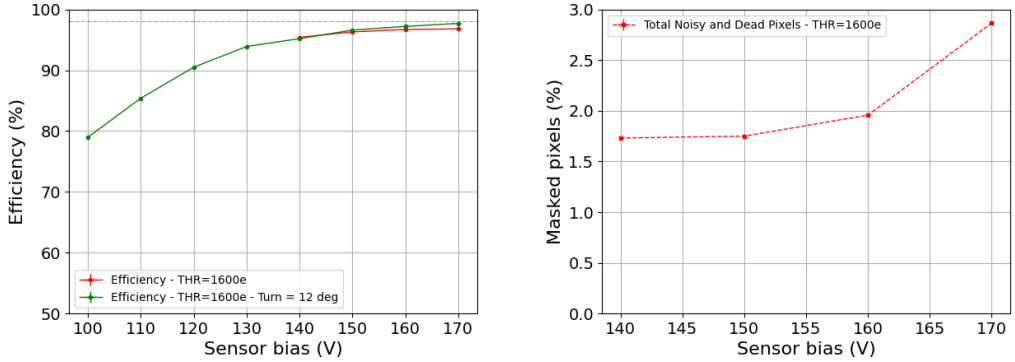

Fig. 11. Plots showing the efficiency (left) and percentage of masked pixels (right) for irradiated FBK sensors at 1.8×10^{16} n_{eq}/cm^2, as a function of the sensor bias voltage. In the plot on the left are reported measurements with tracks at normal incidence (red), and with tracks at 12-degree incidence angle (green). The efficiency does not include the masked pixels. The average threshold was 1600 electrons.

fluences of $2.1 \pm 0.08 \times 10^{16}$ n_{eq}/cm^2 and $2.6 \pm 0.09 \times 10^{16}$ n_{eq}/cm^2 for the first and second samples, respectively. The uniformity was measured as the standard deviation of the fluence in the ROI, and was found to be 0.03. In each ROI, and for both samples, we measured the efficiency and the average cluster size as a function of the sensor bias voltage, as reported in Fig. 12.

At the highest sensor bias voltage we measured an efficiency of 92% (90%) and a masked pixel percentage of 7% (< 4%) for the 2.1 (2.6) $\times 10^{16}$ n_{eq}/cm^2 sensor. Also, in this case we masked all pixels with a noise occupancy greater than 2×10^{-5}.

8. Summary

Qualification of 3D silicon pixel sensors for the High Luminosity upgrade of the CMS Inner Tracker is progressing well. 3D sensors have been irradiated up to 2.6×10^{16} n_{eq}/cm^2. Their performance are quite good in terms of efficiency and resolution. We observe a large increase of noisy pixels as as function of the sensor bias voltage for fluences greater than 1.5×10^{16} n_{eq}/cm^2, which is under investigation. Our plan is to perform the same measurements presented in this article with

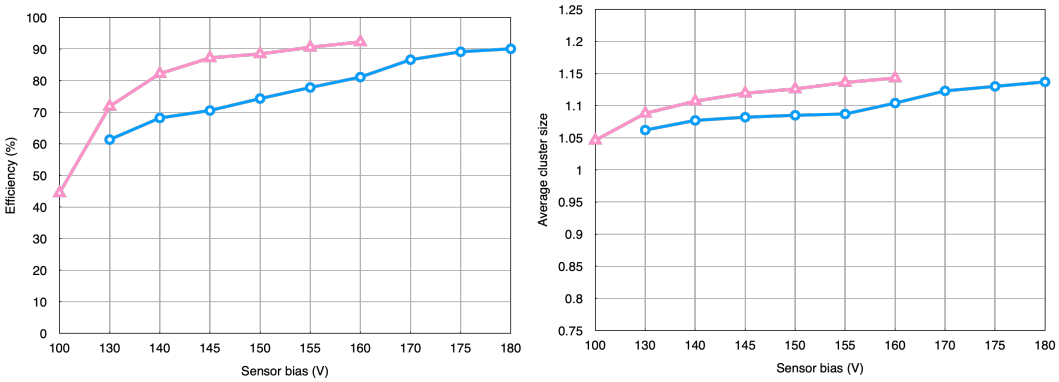

Fig. 12. Plots showing the efficiency (left) and average cluster size (right) for irradiated FBK sensors, at 2.1×10^{16} n_{eq}/cm^2 (pink) and 2.6×10^{16} n_{eq}/cm^2 (blue), as a function of the sensor bias voltage. The efficiency does not include the masked pixels. The average threshold was 2000 electrons and 1900 electrons for the lower and highly irradiated samples, respectively.

the final version of the readout chip, in order to finalize, by next year, our strategy for barrel layer 1 during the HL-LHC era.

References

[1] F. Baggins et al., "High-Luminosity Large Hadron Collider (HL-LHC): Preliminary Design Report", CERN-2015-005 (2015).

[2] CMS Collaboration, "The Phase-2 Upgrade of the CMS Tracker", CERN-LHCC-2017-009 and CMS-TDR-014 (2017).

[3] RD53 Collaboration, "RD Collaboration Proposal: development of pixel readout integrated circuits for extreme rate and radiation", CERN-LHCC-2013-008 and LHCC-P-006 (2013).

[4] R. Diener at al., "The DESY II test beam facility", Nucl. Instrum. Meth. A **922** (2019) 265-286.

[5] Fondazione Bruno Kessler (FBK) web site https://sd.fbk.eu

[6] Centro Nacional de Microelectronica (CNM) web site http://www.cnm.es

[7] Karlsruhe Institute of Technology (KIT) web site https://www.kit.edu

[8] IceMos Technology, Belfast, web site https://icemostech.com

[9] Gian-Franco Dalla Betta at al., "Development of a new generation of 3D pixel sensors for HL-LHC", Nucl. Instrum. Meth. A **824** (2016) 386-387.

[10] Gian-Franco Dalla Betta at al., "The INFN–FBK Phase-2 R&D program", Nucl. Instrum. Meth. A **824** (2016) 388-391.

[11] Hendrik Jansen at al., "Performance of the EUDET-type beam telescopes", EPJ Techn. Instrum. **3** (2016) 7.